JAM CM Journal of Applied Mathematics and Computational Mechanics 2024, 23(3), 130-138
www.amcm.pcz.pl p-ISSN 2299-9965
DOI: 10.17512/jamcm.2024.3.12 e-ISSN 2353-0588

FINITE ELEMENT ANALYSIS OF THE SINGLE SHEAR PIERCING PUNCH PERFORMANCE FOR BELT PERFORATION

Dominik Wojtkowiak, Krzysztof Talaśka

Institute of Machine Design, Faculty of Mechanical Engineering, Poznan University of Technology
Poznań, Poland
dominik.wojtkowiak@put.poznan.pl

Received: 31 July 2024; Accepted: 13 September 2024

Abstract. Modification of the punch geometry can greatly reduce the force necessary to perform the perforation of the belt. This paper presents research on the asymmetrical single sheared piercing punch. FEM analysis was performed for a variable shear angle α in range of 5-45° for constant punch diameter D = 10 mm and a TFL10S belt. Based on the obtained results, the influence of the shear angle on the perforation force F_P, punch deflection f and pneumatic cylinder stroke increase Δs was determined. FEM analysis was divided into two stages: the dynamic one, which was used to obtain the perforation force in function of punch displacement characteristics, and the static one, which helped to establish the deflection of the punch for the peak value of the perforation force. Additionally, the application of the obtained results is presented for the punching die design process when the effective geometrical features of the tools are desired.

MSC 2010: *74B99, 74R99*
Keywords: *piercing punch, belt perforation, tool optimization, FEM, asymmetrical punch, single shear punch*

1. Introduction

Modifications to the punch geometry can significantly reduce the force required to create holes in the material [1, 2]. One of the methods is to perform the shearing of the punch [3], which creates the asymmetrical tool – single sheared punch (Fig. 1). It is beneficial to metal processing [4] and other rigid materials [5-7], but its performance has not been tested in multilayer polymer composite belts (Fig. 2).

Belt punching with two cutting edges is a relatively complex problem. Due to the orthotropic mechanical properties of multilayer polymer composite belts, conventional punching theory is not always suitable for such applications. There are some similarities in the behaviour of non-classical materials [8, 9] and natural polymers [10, 11]. In addition to mechanical properties, chemical compounds and thermal mechanical properties may affect the process of machining [12-15].

The aim of the study is to investigate the influence of the shearing angle α on the perforation force F_P, punch deflection f and pneumatic cylinder stroke increase Δs. This information may be useful during the design process of punching dies for belt perforation. Applying design assumptions and limitations allows one to optimize the tool geometry to achieve a functional machine construction. The last of the analysed parameters especially have an impact on selecting the proper drive and positioning method, which also affects the efficiency of the process.

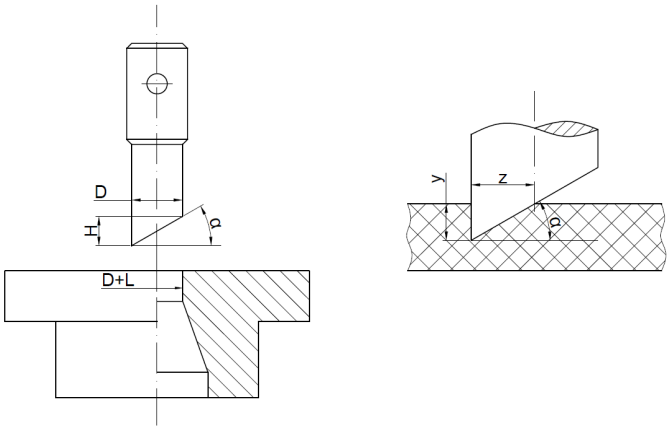

Fig. 1. Single shear punch cooperating with a die: D – punch diameter, H – shearing height, L – punch-die clearance, α – shear angle

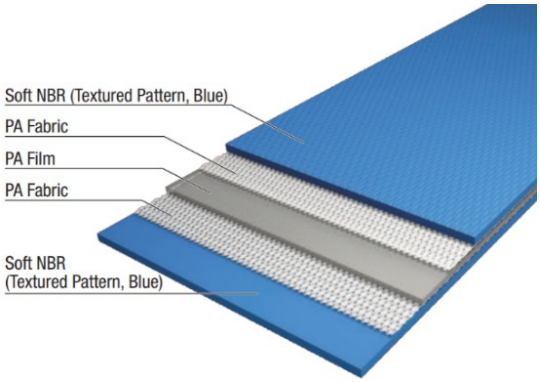

Fig. 2. Multilayer polymer composite belt [16]

2. Methodology of research

During the research, the main focus was put on the FEM analysis in ABAQUS 6.13 software. It is widely used to improve either the design of the machines [17, 18] or the manufacturing process [19, 20]. The advantage of this approach is that it is not required to make a set of tools with various shear angles [1-3]. However, validation of the model requires at least a single experimental result to compare in order to

verify the correctness of the applied modelling methodology. The experimental results for such punch geometry was presented in [1].

In this research, the FEM analysis was divided into two stages: the dynamic one, which was used to obtain the characteristics of perforation force in function of punch displacement, and the static one, which helped to established the deflection of the punch for the peak value of the perforation force. The construction of both FEM models is presented in Figure 3a and 3b, respectively.

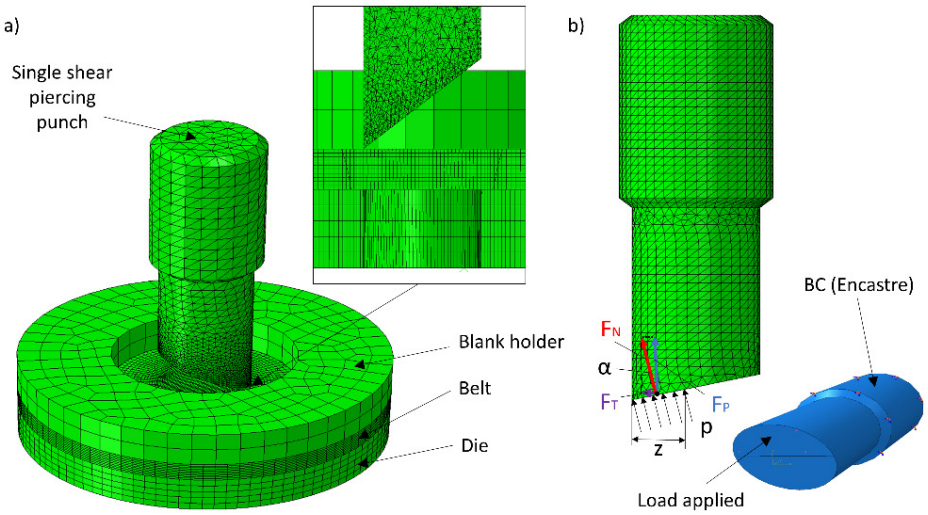

Fig. 3. FEM model construction

In the ABAQUS Explicit model (Fig. 3a), the belt is modelled as a deformable part, while the rest of the instances (punch, die and blank holder) are treated as rigid objects. The stiffness of the belt is much smaller than the steel tools, which makes it possible to use such simplification. It greatly reduces the computational time of the analysis. The kinematic extortion of the punch was provided by the boundary condition of the velocity in the Z axis of 0.5 mm/s. Using such velocity provides a quasi-static characteristic of the analysed process, which eliminates the influence of the strain rate and makes it possible to use mass scaling without affecting the results. The perforation force is read from the reference point of the punch as a $F_P(t)$ characteristic. In order to adjust the moment of belt failure, the damage evolution has to be defined with proper displacement at failure. Since changing the punch geometry has an impact on the mesh, and as a consequence on this value, it has to be established for each single case. The methodology to do it is to choose the value which provides the belt failure when the whole cutting edge of the punch meets the cutting edge of the die. Beside the piercing punch, all the instances were meshed with explicit hexahedral, 3D stress, and linear C3D8R elements. The belt was divided into two parts, so that both cutting edges were in contact with the same element. Due to the complex geometry, the tetrahedral C3D10M element was used to mesh the grip part

of the punch. The mesh control used in the model allows 10 elements to be obtained on the thickness belt of 0.00026 m each. It also provides the dense mesh in the region near the shear section. In the case of the belt instance, the deletion of elements has been enabled.

The tests were conducted for the TFL10S belt, whose construction is similar to the one presented in Figure 2. This belt is characterized by increased strength and high rigidity, which indicates that it is hard to perforate, making it a reasonable choice as the test material. The belt thickness is $t = 2.65$ mm, while its polyamide core is 1 mm thick. Parameters necessary to model the belt properties and its damage in the FEM model are presented in Table 1 and were determined based on the previous research [1, 2]. Although the belt should be considered an orthotropic material, the simplification of using the parameters of an isotropic substitute and the Johnson-Cook damage model was explained and justified in [1, 2, 21].

According to the ABAQUS documentation, the Johnson-Cook plasticity model is suitable only for high-strain-rate deformation of metals, but it was proved that it can be adapted for damage modelling in the belt punching process [1, 2, 21].

The Johnson-Cook dynamic failure model is made on the basis of value of the equivalent plastic strain at element integration points. It is assumed that the failure occurs when the damage parameter exceeds 1. The definition of damage parameter ω is as following:

$$\omega = \sum \left(\frac{\Delta \bar{\varepsilon}^{pl}}{\bar{\varepsilon}_f^{pl}} \right) \tag{1}$$

where $\Delta \bar{\varepsilon}^{pl}$ is an increment of the equivalent plastic strain, $\bar{\varepsilon}_f^{pl}$ is the strain at failure, and the summation is performed over all increments in the analysis. The strain at failure, $\bar{\varepsilon}_f^{pl}$, is assumed to be dependent on a nondimensional plastic strain rate, $\dot{\bar{\varepsilon}}^{pl}/\dot{\varepsilon}_0$ a dimensionless pressure-deviatoric stress ratio p/q (where p is the pressure stress and q is the Mises stress) and the nondimensional temperature, $\hat{\theta}$. The dependencies are assumed to be separable and are of the form:

$$\bar{\varepsilon}_f^{pl} = \left[d_1 + d_2 \cdot \exp\left(d_3 \frac{p}{q} \right) \right] \cdot \left[1 + d_4 \cdot \ln\left(\frac{\dot{\bar{\varepsilon}}^{pl}}{\dot{\varepsilon}_0} \right) \right] \cdot \left(1 + d_5 \hat{\theta} \right) \tag{2}$$

where d_1-d_5 are failure parameters measured at or below the transition temperature and provided by the user when defining the Johnson-Cook dynamic failure model. The simplified model (created by neglecting the d_4 and d_5 parameters connected with changing the temperature $\hat{\theta}$ and strain rate $\dot{\varepsilon}_0$) was used for the computational modelling in this research, as presented below:

$$\bar{\varepsilon}_f^{pl} = d_1 + d_2 \cdot \exp\left(d_3 \frac{p}{q} \right) \tag{3}$$

If this failure criterion is met, the deviator stress components will be set to zero and remain zero for the rest of the analysis. Depending on the chosen option, the pressure stress can also be set to zero for the rest of the calculation, which means that this element will be deleted from analysis, or it may remain in the analysis as the compressive one. In the presented study, the first option was chosen.

Table 1. Mechanical properties of the TFL10S belt used for FEM modelling

Density ρ [kg/m^3]	Young's Moduli E [MPa]	Poisson ratio ν [–]	Johnson-Cook model parameters				
			d_1	d_2	d_3	d_4	d_5
1140	235	0.2	–0.24	0.32	2.6	0	0

To determine the test range of the variable shear angle, the correlation between the geometrical parameters of the punch and the shear angle α was specified (Fig. 1):

$$\tan\alpha = H/D \rightarrow \alpha = \arctan(H/D) \tag{4}$$

In order to maintain the constant mechanical cutting work during the process and prevent the closed-contour punching to obtain the most effective force reduction, we can assume that the shearing height H should be greater or equal to the belt thickness t. For a punch with diameter D = 10 mm, the minimal shear angle α should be greater than 15°. Based on that, in this research, two shear angles below this value and a few greater than the estimated value are considered. Tests were performed for shear angle α = 5°, 10°, 15°, 20°, 25°, 30° and 45°.

For punch deflection analysis (Fig. 3b), the model contains only a single instance – the punch. The greatest deflection should occur for the peak value of the force, which can be obtained from the dynamic FEM analysis and the punch displacement x very close to the belt thickness t. Because for the shear angles greater than 15°, the contact area between the punch and belt where the force will be distributed does not cover the whole front surface in the specific moment of time for which $x = t$, and it may cause the eccentricity of the resultant compression force. It will generate an additional bending moment, which increases the deflection of the punch. In order to model it, the partition on the front surface of the punch was created and the pressure was applied to its surface. To define its size, the z value was calculated (Table 2) with the following equation:

$$\tan\alpha = y/z \rightarrow z = (y \cdot D)/H \tag{5}$$

Because the pressure is applied in the normal direction to the front surface of the punch, it is necessary to determine the normal force, according to the following equation:

$$\cos\alpha = F_P/F_N \rightarrow F_N = F_P/\cos\alpha \tag{6}$$

Table 2. Dimensions of the pressure area on the front surface of the single sheared punch

Shear angle α [°]	5	10	15	20	25	30	45
z [mm]	10	10	9.88	7.28	5.68	4.59	2.65

For the empirical testing used in model validation, the MTS Insight 50 kN strength testing machine was used. During the tests, five holes spaced 20 mm were made in the rectangular specimen 30 × 150 mm with the speed of traverse 0.5 mm/s, in order to maintain the quasi-static nature of the research. During the measurements, the force and displacement of the punch were recorded as $F(x)$ characteristics.

3. Results and discussion

The comparison of the FEM and experimental results for TFL10S belt perforation with a single shear punch with a shear angle $\alpha = 30°$ is presented in Figure 4. As can be observed, the divergence of the characteristics is significant. The reason for that is the impossibility of modelling the phenomena which occur in the middle of the experimental curve with such a simplified damage model. However, the peak value does not lie too far from the experimental one – for FEM $F_{PMAX} = 1694$ N and for experimental tests $F_{PMAX} = 1847$ N. This indicates that the proposed model is not appropriate for the force characteristic approximation and can be simply used for the estimation of the peak force tendency for various tool geometry.

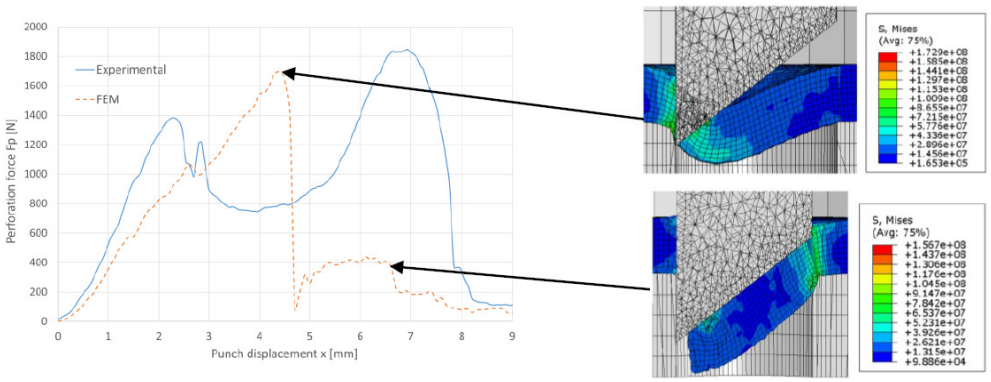

Fig. 1. Comparison of FEM and experimental results for TFL10S belt perforation with a single shear punch with a shear angle $\alpha = 30°$ along with sample stress distribution obtained from FEM analysis

The results are presented in Table 3. Based on these results, the characteristics showing the influence of the shear angle α on the perforation force F_P, punch deflection f and pneumatic cylinder stroke increase Δs were derived (Fig. 5).

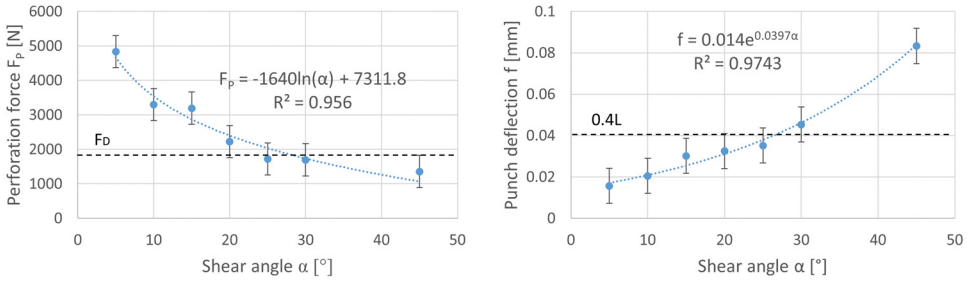

Fig. 5. The influence of the shear angle on the perforation force F_P and the punch deflection f

Table 3. FEM analysis results for the single sheared punch during TFL10S belt perforation

Shear angle α [°]	Perforation force F_P [N]	Punch deflection f [mm]	Stroke increase Δs [mm]
5	4832	0.0156	0.87
10	3293	0.0205	1.76
15	3212	0.0301	2.68
20	2224	0.0325	3.64
25	1719	0.0351	4.66
30	1694	0.0453	5.77
45	1355	0.0833	10

As can be observed, there is a negative exponential correlation between the shear angle α and the perforation force F_P. On the other hand, the positive, non-linear correlation between the shear angle and the punch deflection f is visible. Since the correlation is reverse, it is possible to find the effective solution by applying constructional restrictions to the obtained models and find the shear angle range α which fulfills both conditions.

If we assume that the drive for the designed punching die is the pneumatic cylinder with piston diameter d = 63 mm and operates under pressure of 6 bars, the drive force F_D = 1870 N. For belt perforation, we use a very small punch-die clearance L = 0.1 mm, which indicates that the deflection cannot exceed 0.5L (for assurance that no asperity contact between the punch and die occurs, causing tool wear or damage, we can take 0.4L). Increasing the stroke has a negative effect on the life of the return springs in the punching die, so it should also be limited. If we apply the above-mentioned assumptions to the characteristics in Figure 5, we only have a very narrow range of shear angles where the value of α = 25 ° lies. For this value the stroke increase Δs is 4.66 mm, so it would greatly reduce the life of the return springs. As can be observed, it is very hard to find the effective solution for a single sheared punch for belt perforation and for some sets of design parameters, it may be impossible.

4. Conclusions

Based on the obtained results, we can conclude that using a single sheared punch can greatly reduce the perforation force (for a shear angle in range of 5-45° the perforation force varies respectively from 4832 N to 1355 N), however the asymmetry of the punch causes the transverse force, which leads to punch deflection (increaseing the shear angle by 40° may cause over 5-times greater deflection). Since small punch-die clearances are required for belt punching, the shearing of the punch can be only used for a limited range of shear angles α. However, in order to obtain the effective reduction of the perforation force F_P, the shear angle should exceed 15° in order to avoid closed-contour punching. Based on the presented characteristics, it is possible to find a solution which fulfils both criteria, but it is very difficult. For the obtained results and assumed drive force and clearance there is only one solution (25°), but it can be observed that selecting different reference values may lead to no solutions at all. It shows the clear advantage of symmetrical punches over asymmetrical ones for belt perforation.

References

[1] Wojtkowiak, D., Talaśka, K., Malujda, I., & Domek, G. (2018). Estimation of the perforation force for polymer composite conveyor belts taking into consideration the shape of the piercing punch. *Int. J. Adv. Manuf. Technol.*, *98*(9-12), 2539-2561.

[2] Wojtkowiak, D., & Talaśka, K. (2019). Determination of the effective geometrical features of the piercing punch for polymer composite belts. *Int. J. Adv. Manuf. Technol.*, *104*(1-4), 315-332.

[3] Review on Pneumatic Punching Machine and Modification in Punch Tool to Reduce Punching Force Requirement, https://www.harsle.com, last accessed 2024/05/07.

[4] Singh, U.P., Strepel, A.H., & Kals, H.J.J. (1992). Design study of the geometry of a punching/ blanking tool. *J. Mat. Process. Technol.*, *33*, 331-345.

[5] Zain, M.S.M., Abdullah, A.B., & Samad, Z. (2017). Effect of puncher profile on the precision of punched holes on composite panels. *Int. J. Adv. Manuf. Technol.*, *89*, 3331-3336.

[6] Pramono, A.E., Indriyani, R., Zulfia, A., & Subyakto, (2015). Tensile and shear punch properties of bamboo fibers reinforced polymer composites. *Int. J. Composite Mat*., *5*, 9-17.

[7] Yang, T., Hao, J., Liu, G., Su, H.B., Chen X.P., & Qi, Y.B. (2014). Influence of punch shape on the fracture surface quality of hydropiercing holes. *J. Harbin. Inst. Technol*., *21*(3), 85-90.

[8] Górecki, J., Malujda, I., Talaśka, K., Wilczyński, D., & Wojtkowiak, D. (2018). Influence of geometrical parameters of convergent sleeve on the value of limit stress. *MATEC Web of Conferences*, 157, 05006.

[9] Bembenek, M., Kowalski, Ł., Pawlik, J., & Bajda, S. (2022). Research on the influence of the load direction and the cross-section shape on the Young's Modulus of elements produced by the Fused Deposition Modeling Method. *J. Mater. Eng. Perform*., *31*, 7906-7912.

[10] Wilczyński, D., Wałęsa, K., Berdychowski, M., & Kukla, M. (2020). Biomass cutting tests to determine the lowest value of the process force. *IOP Conf. Ser.: Mater. Sci. Eng.*, 776, 012014.

[11] Wilczyński, D., Talaśka, K., Wojtkowiak, D., Górecki, J., & Wałęsa, K. (2024). Research on energy consumption of the biomass cutting process as a process preceding biofuel production. *Biosyst. Eng.*, *237*, 142-156.

[12] Wałęsa, K., Malujda, I., & Wilczyński, D. (2020). Experimental research of the thermoplastic belt plasticizing process in the hot plate welding. *IOP Conf. Ser.: Mater. Sci. Eng.*, *776*, 012011.

[13] Domański, T., Piekarska, W., Saga, M., Kubiak, M., Saternus, Z., & Sagova, Z. (2023). Influence of thermal loads on the microstructure and mechanical properties of structural steel. *Acta Phys. Pol. A*, *144*(5), 300-303.

[14] Bembenek, M., & Uhryński, A. (2022). The use of thermography to determine the compaction of a saddle-shaped briquette produced in an innovative roller press compaction unit. *AMA*, *16*(4), 340-346.

[15] Wałęsa, K., Malujda, I., & Wilczyński, D. (2019). Shaping the parameters of cylindrical belt surface in the joint area, *AMA*, *13*(4), 255-261.

[16] XH series for Folder Gluer Machine, www.nitta.de, last accessed 2024/05/07.

[17] Dudziak, M., Domek, G., Kołodziej, A., & Talaśka, K. (2014). Contact problems between the hub and the shaft with a three angular shape of cross-section for different angular positions. *Procedia Eng.*, *96*, 50-58.

[18] Fierek, A., Malujda, I., Wilczyński, D., & Wałęsa, K. (2020). Analysis of shaft selection in terms of stiffness and mass. *IOP Conf. Ser.: Mater. Sci. Eng.*, 776, 012028.

[19] Wałęsa, K., Biszczanik, A., Malujda, I., & Wilczyński, D. (2022). Assumptions for modeling of the hot plate welding process considering the automatic welding machine design. *MATEC Web of Conferences*, 357, 05002.

[20] Domański, T., Piekarska, W., Saternus, Z., Kubiak, M., & Stano, S. (2022). Numerical prediction of strength of socket welded pipes taking into account computer simulated welding stresses and deformations. *Materials*, *15*(9), 3243.

[21] Talaśka, K., & Wojtkowiak, D. (2018). Modelling mechanical properties of the multilayer composite materials with the polyamide core. *MATEC Web of Conferences*, 157, 02052.